Scripta Materialia 178 (2020) 295–300

Contents lists available at ScienceDirect

Scripta Materialia

journal homepage: www.elsevier.com/locate/scriptamat

Deactivating deformation twinning in medium-entropy CrCoNi with small additions of aluminum and titanium

C.E. Slone[a,b,*], C.R. LaRosa[b], C.H. Zenk[a,b], E.P. George[c,d], M. Ghazisaeidi[b], M.J. Mills[a,b]

[a] Center for Electron Microscopy and Analysis, The Ohio State University, Columbus, OH, 43212, USA
[b] Department of Materials Science and Engineering, The Ohio State University, Columbus, OH 43210, USA
[c] Materials Science and Technology Division, Oak Ridge National Laboratory, Oak Ridge, TN 37831, USA
[d] Materials Science and Engineering Department, University of Tennessee, Knoxville, TN 37996, USA

ARTICLE INFO

Article history:
Received 12 October 2019
Revised 21 November 2019
Accepted 23 November 2019
Available online 3 December 2019

Keywords:
Medium- and high-entropy alloys
CrCoNi alloy
TWIP steel
Deformation twinning
Work-hardening

ABSTRACT

High strain-hardening rates in equiatomic CrCoNi and other multi-principal element alloys have been attributed to deformation twinning. This work shows that small additions of Al and Ti to a CrCoNi alloy deactivate deformation twinning with only minor changes to uniform elongation and ultimate tensile strength. The initial microstructure is free of chemically ordered (Al,Ti)-rich precipitates after solutionizing and quenching. Tensile properties for the alloy are reported and compared to equiatomic CrCoNi, and the post-deformation microstructure is assessed. Density functional theory calculations indicate that energetically unfavorable Al-Al bonds may discourage shearing via partial dislocations, which are necessary for twinning to occur.

Recent interest in medium- and high-entropy alloys is due to their excellent mechanical properties, including high strength, large uniform and total elongations, high strain-hardening rates, and good fracture toughness [1–5]. In common face-centered cubic high-entropy alloys like equiatomic CrMnFeCoNi, and its medium-entropy subsets, such as CrFeCoNi and CrCoNi, these properties have been attributed to low stacking fault energies that promote planar slip, deformation twinning, and in some cases, deformation-induced phase transformations [6–9]. Twinning-induced plasticity (TWIP) and transformation-induced plasticity (TRIP) effects are also well-known in high-Mn steels, which exhibit similar properties to the medium- and high-entropy alloys noted above [10–13]. In both classes of alloys, and in emerging alloys inspired by both HEAs and TWIP / TRIP steels, the relationships among composition, stacking fault energy, and deformation mechanisms have been scrutinized as a means for more deliberate engineering in future alloy development [14–16].

The medium-entropy, equiatomic CrCoNi system embodies the outstanding mechanical properties described above, and displays simultaneous improvements to strength and ductility at cryogenic temperatures [6,9,17]. At room temperature and small strains, plasticity occurs through shearing of $a/6\langle 112\rangle$ partial dislocations with typical separations on the order of ~6–14 nm [18], which is consistent with a low intrinsic stacking fault energy of approximately 18–22 mJ/m^2 [6,9,18]. Larger deformations lead to mechanical twinning. Although twinning contributes only modestly to elongation (at most about 5% tensile strain), it is commonly believed to generate the exceptionally high strain-hardening rates observed in CrCoNi [9,19]. This is hypothesized to occur through the same dynamical Hall-Petch effect that is nominally active in TWIP steels [10,20].

Given the apparent role of twinning in a variety of alloys (including CrCoNi, other HEAs based on the CrFeMnCoNi system, and TWIP steels), it is important to explore how changes in composition affect the propensity for twinning and, therefore, macroscopic mechanical behavior. Recent efforts have explored the influence of substitutional elements such as Nb [21], W [22], Mo [23,24], Al [25–27], and Ti [28] on the mechanical properties of the CrCoNi system. However, it is currently unclear whether and to what extent these affect the underlying deformation mechanisms. In this work, we show that small additions of Al and Ti can deactivate deformation twinning in CrCoNi, and that this has surprisingly little impact on the hardening rate and uniform elongation of the new alloy.

The composition of the alloy (V1) used to demonstrate this is shown in Table 1 and combines alloying principles from equiatomic CrCoNi and Inconel 740H, a Ni-base superalloy highly enriched in Cr and Co [29]. A thorough exploration of the design

* Corresponding author.
E-mail address: slone.103@osu.edu (C.E. Slone).

https://doi.org/10.1016/j.scriptamat.2019.11.053
1359-6462/

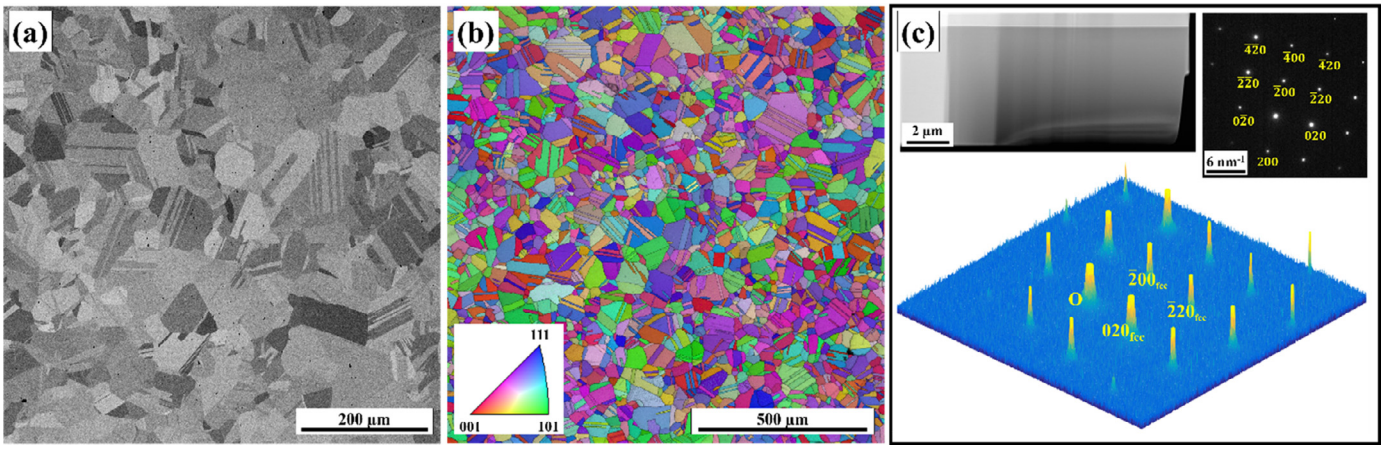

Fig. 1. Initial microstructure of alloy V1 in the fully recrystallized and solutionized condition. (a) BSE image showing single phase grain structure with annealing twins. (b) Inverse pole figure showing minimal recrystallization texture. (c) Inset shows an extracted FIB foil near a ⟨001⟩ normal orientation and the absence of any fine-scale precipitates. Selected area diffraction pattern showing a single-phase fcc structure and the absence of ordered γ' superlattice reflections.

Table 1
Compositions of new alloy V1 and its parent alloys, equiatomic MEA CrCoNi and Ni-base superalloy Inconel 740H.

Alloy		Ni	Cr	Co	Al	Ti	Nb	Mo
740H	**Wt.%**	Bal (24.5)	24.5	20	1.35	1.35	1.5	0.1
	At.%	49.0	26.5	19.1	2.8	1.6	0.9	0.1
CrCoNi	**Wt.%**	34.7	30.6	34.7	–	–	–	–
	At.%	33.4	33.3	33.3	–	–	–	–
V1	**Wt.%**	32.7	28.6	33.2	2.0	2.0	1.5	–
	At.%	31.0	30.6	31.3	4.1	2.3	0.9	–

Totals may not sum to 100% due to rounding errors.

Table 2
Grain size and mechanical properties of alloy V1 and equiatomic CrCoNi.

	CrCoNi	V1
Grain size (μm)	24	59
Yield strength (MPa)	346	350
Tensile strength, σ_{true} (MPa)	1307	1231
Uniform elongation, ε_{true} (MPa)	0.43	0.42
Total elongation (ε_{true})	0.57	0.48
Total elongation (ε_{engr})	0.76	0.62

rationale, stability, and aging response of V1 has previously been reported [30]. Additional details regarding alloy fabrication are also described in that work.

Alloy V1 was cast, homogenized / solutionized, quenched, and cold rolled. To facilitate a direct comparison with equiatomic CrCoNi, which is a single-phase, solid solution alloy, tests of alloy V1 in this work were performed following an additional solutionizing and quenching treatment. Solutionizing was performed at 1323 K (1050 °C) and followed by rapid quenching in water to prevent precipitation of the (Al,Ti)-rich γ' phase. This also induced full recrystallization after the prior cold rolling step.

Microstructures were studied using a Thermofisher Scientific Apreo scanning electron microscope (SEM) and a Tecnai F20 200 kV S/TEM. Grain size was measured using the linear intercept method [31] with backscattered electron images, and texture and annealing twins were identified using electron backscatter diffraction (EBSD) orientation mapping. Scans were acquired using an accelerating voltage of 20 kV and a beam current of 6.4 nA with a step size of 2 μm. To search for precipitation in the as-quenched microstructure, selected area diffraction patterns were acquired via parallel beam transmission electron microscopy.

The initial microstructure of alloy V1 is shown in Fig. 1. Except for incidental Ti-rich carbides, the alloy was a fully recrystallized, single phase solid solution with an average grain size of 59 ± 2.5 μm (standard error). The backscattered electron image of Fig. 1a shows abundant annealing twins, similar to equiatomic CrCoNi. Annealing twins are also visible in the inverse pole figure map of Fig. 1b, which shows the fully recrystallized microstructure and absence of a strong recrystallization texture. As described more thoroughly in previous work [30], the single-phase nature of the alloy after quenching was confirmed by X-ray diffraction (not shown here) and conventional transmission electron microscopy. A ⟨100⟩ zone axis selected area diffraction pattern is shown in Fig. 1c with a corresponding intensity plot. Since Al and Ti strongly promote precipitation of the chemically ordered γ' phase, which is commonly used to impart high-temperature strength to Ni-base superalloys, the absence of ordered superlattice reflections in Fig. 1c confirms that alloy V1 consists of a single, face-centered cubic phase like equiatomic CrCoNi.

Tensile testing of alloy V1 was performed on an electro-thermal mechanical tester (ETMT) using sub-size specimens (nominal gauge dimensions 5 mm length × 2 mm width × 1 mm thickness) and a nominal strain rate of 10^{-3} s^{-1}. Engineering stress-strain curves for alloy V1 and equiatomic CrCoNi are shown in Fig. 2a, and a comparison to equiatomic CrCoNi (previously tested with the same sample geometry and experimental setup [19]) is shown in Table 2. Both alloys have very similar yield strengths of approximately 350 MPa, although it should be noted that the grain size is considerably larger in alloy V1 (59 μm) compared to CrCoNi (~24 μm). For the same grain size, alloy V1 would be expected to have a higher yield strength than CrCoNi.

Alloy V1 exhibited substantial work hardening to achieve an ultimate true tensile strength of 1231 ± 44 MPa. Although this is approximately 80 MPa less than the tensile strength of equiatomic CrCoNi, the uniform elongation of both alloys was nearly identical (0.42 ± 0.03 in alloy V1 and 0.43 in CrCoNi, ε_{true}). However, the total elongation in alloy V1 (0.62 ± 0.06, ε_{engr}) was much lower than in CrCoNi (0.76, ε_{engr}). This behavior can be rationalized in the context of the deformation mechanisms of alloy V1. The microstructure following tensile deformation to failure is shown in Fig. 3.

As previously observed in CrCoNi [19], alloy V1 undergoes substantial texture evolution during deformation and develops a strong ⟨111⟩ - ⟨100⟩ double-fiber texture parallel to the tensile axis, as shown via EBSD measurement in Fig. 3a (step size 1 μm).

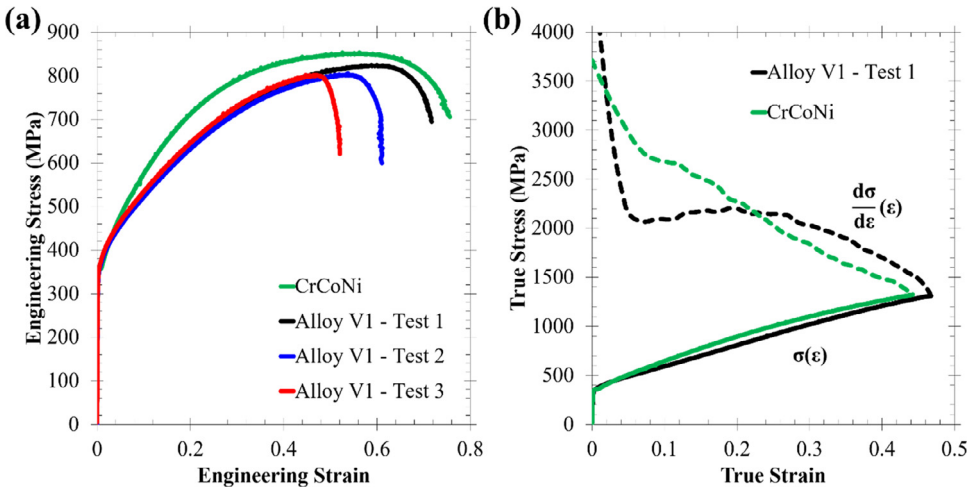

Fig. 2. Tensile response of alloy V1 and equiatomic CrCoNi. (a) Engineering stress-strain curves for three tests. (b) Curves for the true stress-strain response (solid) and work-hardening rate, $d\sigma/d\varepsilon$ (dashed).

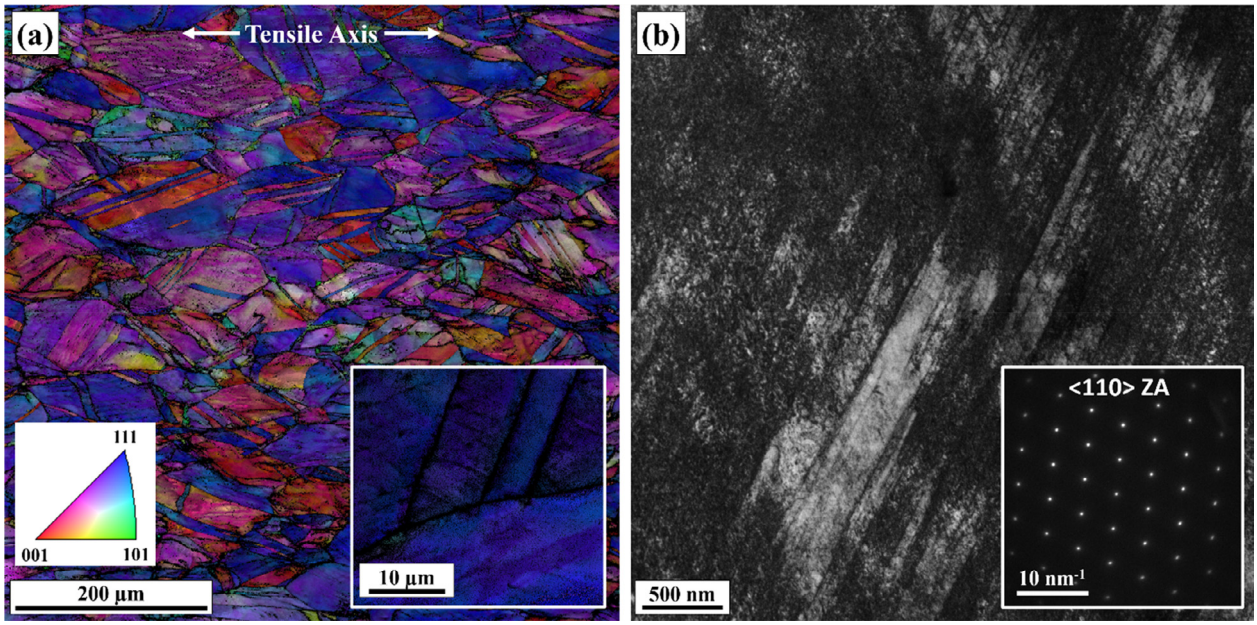

Fig. 3. Microstructure of the fully recrystallized and solutionized condition following tensile deformation to failure. (a) Inverse pole figure map showing the development of a strong ⟨111⟩ and ⟨100⟩ double-fiber texture. Orientations displayed are relative to the tensile axis. (b) ⟨110⟩ zone axis bright-field CTEM showing high dislocation density walls. The inset zone axis selected area diffraction pattern indicates that deformation twins are not present.

However, unlike in CrCoNi, no deformation twins were observed in alloy V1 even with EBSD step sizes as fine as 50 nm (Fig. 3a, inset). This is an important difference between the alloys since deformation twins can be indexed in CrCoNi with EBSD step sizes as coarse as 500 nm, and they are easily sampled with step sizes of 50–100 nm. Although there is an orientation dependence to the prevalence of twinning in CrCoNi [19], even favorably oriented grains (with ⟨111⟩ parallel to the tensile axis) in alloy V1 did not exhibit twins. Dark, un-indexed lines were visible with fine step sizes (Fig. 3a, inset), but parallel beam TEM revealed these to be bands of extremely high dislocation density. Fig. 3b shows a typical example of this with an inset ⟨110⟩ zone axis selected area diffraction pattern from the same region. The absence of reflections about the 111 diffraction spots indicates that deformation twins were not present. Although the inset in Fig. 3b corresponds to a selected area aperture size of 10 µm for optimal image quality, no twin reflections were observed even with larger aperture sizes up to 200 µm.

The absence of deformation twinning in alloy V1 is surprising given its prominence in CrCoNi, CrFeCoNi, and the late stages of deformation in CrMnFeCoNi. However, previous work in Inconel 740H, which inspired the composition of alloy V1, has indicated deformation twinning is inactive in that alloy in a solutionized and quenched condition [32]. This difference in deformation mechanisms may explain disparities in the mechanical response of alloy V1 and CrCoNi. For example, as noted above, the ultimate true tensile strength of alloy V1 is approximately 80 MPa lower than in CrCoNi, a modest decrease of about 6%. Given the similarity in yield strengths, this indicates that average hardening rates are slightly higher in CrCoNi than in alloy V1, which might be attributable to the activation of mechanical twinning and the dynamical Hall-Petch effect. However, the uniform elongation of the two alloys was essentially identical. These observations directly show that substantial work hardening and excellent uniform elongation can be achieved in the absence of deformation twinning, and call into question the necessity of twinning to obtain these properties.

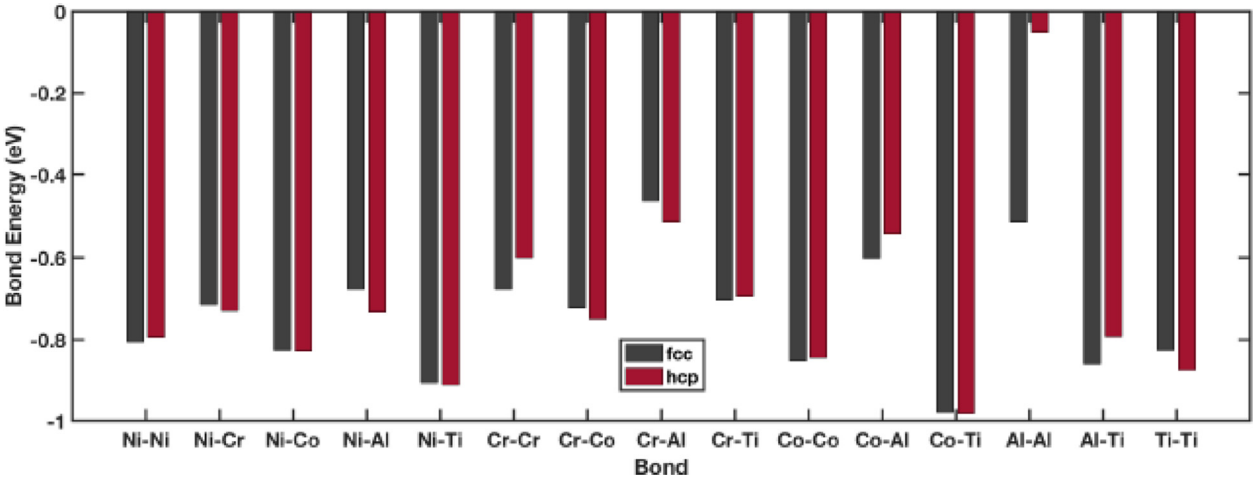

Fig. 4. Pairwise bond energies of components in alloy V1 from DFT calculations. More negative bond energies indicate greater stability for a given pair. The results are shown for both face-centered cubic (gray) and hexagonal close-packed (red) structures.

A more significant difference between CrCoNi and alloy V1 involves the ability to delay fracture after the onset of specimen necking, as defined by the well-known Considere criterion, $d\sigma/d\varepsilon = \sigma_{true}$ [33]. Compared on the basis of true strain, the interval between the onset of necking and fracture was 0.14 in CrCoNi, but only 0.06 in alloy V1. Recent work in the CrMnFeCoNi system suggests that nano-scale deformation twins may provide substantial extrinsic toughening by bridging cracks [2]. This is one plausible reason that despite having very similar uniform elongations, alloy V1 fails much more quickly than CrCoNi after the onset of necking.

Since deformation twinning occurs in CrCoNi at true stresses around 790 MPa, the absence of deformation twinning with minor additions of Al and Ti requires explanation [9,34]. It is well-known that even dilute additions of Al and Ti to Ni-base alloys can result in precipitation of the ordered γ' phase, which discourages room-temperature shearing via $a/6\langle 112\rangle$ partial dislocations; deformation is instead accommodated by single and paired $a/2\langle 110\rangle$ dislocations in γ and γ' [35]. Individual partial dislocations with $a/6\langle 112\rangle$ Burgers vectors produce very unfavorable complex stacking faults in γ' with both incorrect atomic stacking and incorrect atomic neighbors in the chemically ordered structure. Critically, partial dislocations seem to be necessary for deformation twinning to occur, so the presence of γ' could plausibly deactivate twinning by deactivating $a/6\langle 112\rangle$ slip [13,36–38]. However, as shown in Fig. 1, no γ' is present in alloy V1 following solutionizing and quenching, so this explanation is insufficient for the current work.

To better understand the interaction of Al and Ti with Cr, Co, and Ni, density functional theory (DFT) calculations were performed to determine bond energies for binary pairs in the CrCoNi + (Al,Ti) alloy system using the Vienna *ab initio* simulation package (VASP) [39]. Projector augmented wave (PAW) [40] potentials are used with the Perdew-Burke-Ernzerhof [41] generalized-gradient approximations for the exchange-correlation functionals. Methfessel-Paxton smearing of 0.2 eV and a plane wave cut-off of 350 eV are used, and collinear spin polarization is enabled. Both the fcc and hcp structures used to generate the bond energies contained 50 atoms each, with Monkhorst Pack 5 × 5 × 5 and Gamma-centered 5 × 5 × 4 k-point meshes, respectively. All fcc and hcp structures used for the bond energy calculations are special quasi-random structures (SQS) [42], generated by the mcsqs program in the ATAT package [43]. Bond energies for each structure are determined by a linear least square fit of the cohesive energy, which is determined by subtracting the free energy of the atoms from the total energy of the structure. For example, for a binary alloy, the cohesive energy of a given structure can be expressed as:

$$E_{coh} = N_{Ni-Ni}E_{Ni-Ni} + N_{Ni-Co}E_{Ni-Co} + N_{Co-Co}E_{Co-Co}$$

Where $N_{i\text{-}j}$ and $E_{i\text{-}j}$ are the number and energy of *i-j* bonds, respectively. By generating multiple structures with different concentrations, the bond energies for a system (e.g. Ni-Co, Ni-Co-Cr-Al-Ti) can be determined.

Despite the lack of ordering, one possibility is that Al and Ti still have preferred atomic neighbors based on bond energies, and that a non-random distribution of those elements occurs even if the fully ordered γ' structure does not develop. Fig. 4 shows DFT calculations for pairwise bond energies of components in alloy V1 in both face-centered cubic and hexagonal close-packed structures. As an illustration of the previous point, at 0 K, Al=Al bonds have higher energy than other binary pairs (e.g., Ni–Al) and should therefore be disfavored. If this trend holds at elevated temperatures, rapid diffusion during solutionizing should promote a structure with approximately the fewest possible number of Al-Al bonds. Rapid quenching should preserve that structure at room temperature, and any subsequent shearing by dislocations is therefore more likely to increase rather than decrease the number of Al-Al bonds. Notably, this argument applies to both perfect and partial dislocations.

The critical aspect of the deactivation of twinning involves the difference in energy between Al-Al bonds in fcc and hcp configurations. As shown in Fig. 4, Al-Al bonds in an fcc structure are unfavorable (−0.518 eV / bond); however, Al-Al bonds in an hcp structure are by far the least favorable configuration of any calculated for this system (−0.051 eV/bond). This may explain a preference for perfect $a/2\langle 110\rangle$ dislocations compared to $a/6\langle 112\rangle$ partial dislocations, since regions between dissociated partial dislocations have local hcp structure. Wider stacking faults are therefore more likely to contain unfavorable hcp Al–Al bonds. Although CrCoNi is a low-SFE alloy, and Ti decreases the SFE in Ni-base superalloys [44,45], alloy V1 may have a very high local stacking fault energy in regions where Al-Al bonds would be formed by shearing. This makes it exceptionally difficult to develop the extended stacking faults that are necessary for nucleation of deformation twins. Further observations are needed to verify this hypothesis, but one important measurement will be the predominant character of dislocations in alloy V1. Rather than the $\langle 112\rangle$-type partial dislocations observed in CrCoNi, this hypothesis predicts predominantly <110>-type perfect dislocations, or very small average dissociation distances between $\langle 112\rangle$ partials.

Recent work in a variety of high-Mn steels and several other medium- and high-entropy alloys has also shown that deformation twinning may not be necessary for high hardening rates and good uniform elongation. Liang et al. [46] and Luo and Huang [47] have shown that strain hardening in Fe-18Mn-1.7Al-0.5Si-0.75C (wt.%) TWIP steel can be attributed to high dislocation density, and that significant hardening occurs even at elevated temperatures when deformation twinning is severely inhibited. Fu et al. also recently presented evidence that massive cross-slip and dislocation interactions, not twinning, were responsible for strain hardening in an Fe-30Mn-3Si-3Al (wt.%) TWIP steel [48]. Alloys with higher SFE, such as high-Mn steels exhibiting microband-induced plasticity (MBIP) [49] or dynamic slip band refinement [50], also have exceptional ductility without twinning and instead rely on very high dislocation densities for hardening. A similar mechanism has also been qualitatively described in two MPE alloys, equiatomic VCoNi [51] and $CoFeNi_2V_{0.5}Mo_{0.2}$ [52], which exhibit high hardening rates without any apparent deformation twinning. However, more work is needed in this area to reconcile these recent findings with abundant evidence showing a strong correlation between deformation twinning and good combinations of strength and ductility.

In conclusion, this work shows that a single-phase CrCoNi alloy containing Al and Ti has similar mechanical properties to equiatomic CrCoNi but does not undergo deformation twinning. This result suggests that twinning may not be necessary to produce the dynamical Hall-Petch effect in CrCoNi or other MEAs/HEAs and TWIP steels. Instead, hardening in alloy V1 originates from very high dislocation densities arranged in planar structures. While density functional theory calculations offer some preliminary insight regarding the absence of twinning, further modeling and experimental work (particularly regarding the dislocation character) are necessary to understand this change in deformation mechanism.

Declaration of Competing Interest

The authors declare that they have no known competing financial interests or personal relationships that could have appeared to influence the work reported in this paper.

Acknowledgments

The National Science Foundation, Division of Materials Research is acknowledged for supporting CES and MJM (thermo-mechanical processing, materials testing and characterization) under contract #DMR-60050072. CES was also supported by the National Science Foundation Graduate Research Fellowship Program Grant No. DGE-1343012. Any opinions, findings, and conclusions or recommendations expressed in this material are those of the authors and do not necessarily reflect the views of the National Science Foundation. CHZ (transmission electron microscopy) acknowledges financial support from the Alexander von Humboldt foundation. The U.S. Department of Energy, Office of Science, Basic Energy Sciences, Materials Sciences and Engineering Division is acknowledged for supporting EPG (materials synthesis). CRL and MG acknowledge the support by the National Science Foundation Grant DMR-1553355 and the computational resources provided by the Ohio Supercomputer Center.

References

[1] A. Gali, E.P. George, Intermetallics 39 (2013) 74–78, doi:10.1016/j.intermet.2013.03.018.
[2] Z. Zhang, M.M. Mao, J. Wang, B. Gludovatz, Z. Zhang, S.X. Mao, E.P. George, Q. Yu, R.O. Ritchie, Nat. Commun. 6 (2015) 10143, doi:10.1038/ncomms10143.
[3] B. Gludovatz, A. Hohenwarter, K.V.S. Thurston, H. Bei, Z. Wu, E.P. George, R.O. Ritchie, Nat. Commun. 7 (2016) 10602, doi:10.1038/ncomms10602.
[4] G. Laplanche, A. Kostka, O.M. Horst, G. Eggeler, E.P. George, Acta Mater 118 (2016) 152–163, doi:10.1016/j.actamat.2016.07.038.
[5] Z. Zhang, H. Sheng, Z. Wang, B. Gludovatz, Z. Zhang, E.P. George, Q. Yu, S.X. Mao, R.O. Ritchie, Nat. Commun. 8 (2017) 14390, doi:10.1038/ncomms14390.
[6] J. Miao, C.E. Slone, T.M. Smith, C. Niu, H. Bei, M. Ghazisaeidi, G.M. Pharr, M.J. Mills, Acta Mater 132 (2017) 35–48, doi:10.1016/j.actamat.2017.04.033.
[7] Q. Lin, J. Liu, X. An, H. Wang, Y. Zhang, X. Liao, Mater. Res. Lett. 6 (2018) 236–243, doi:10.1080/21663831.2018.1434250.
[8] C. Niu, C.R. Larosa, J. Miao, M.J. Mills, M. Ghazisaeidi, Nat. Commun. 9 (2018).
[9] G. Laplanche, A. Kostka, C. Reinhart, J. Hunfeld, G. Eggeler, E.P. George, Acta Mater 128 (2017) 292–303, doi:10.1016/j.actamat.2017.02.036.
[10] S. Allain, J. Chateau, O. Bouaziz, Mater. Sci. Eng. A. 389 (2004) 143–147, doi:10.1016/j.msea.2004.01.060.
[11] S. Allain, J.P. Chateau, O. Bouaziz, S. Migot, N. Guelton, Mater. Sci. Eng. A. 387–389 (2004) 158–162, doi:10.1016/j.msea.2004.01.059.
[12] I. Gutierrez-Urrutia, S. Zaefferer, D. Raabe, Mater. Sci. Eng. A. 527 (2010) 3552–3560, doi:10.1016/j.msea.2010.02.041.
[13] B.C. De Cooman, Y. Estrin, S. Kyu, Acta Mater 142 (2018) 283–362, doi:10.1016/j.actamat.2017.06.046.
[14] Y. Deng, C.C. Tasan, K.G. Pradeep, H. Springer, A. Kostka, D. Raabe, Acta Mater 94 (2015) 124–133, doi:10.1016/j.actamat.2015.04.014.
[15] Z. Li, K.G. Pradeep, Y. Deng, D. Raabe, C.C. Tasan, Nature 534 (2016) 227, doi:10.1038/nature17981.
[16] D. Raabe, Z. Li, D. Ponge, MRS Bulletin 44 (2019) 266–272, doi:10.1557/mrs.2019.72.
[17] Z. Wu, H. Bei, G.M. Pharr, E.P. George, Acta Mater 81 (2014) 428–441, doi:10.1016/j.actamat.2014.08.026.
[18] S.F. Liu, Y. Wu, H.T. Wang, J.Y. He, J.B. Liu, C.X. Chen, X.J. Liu, H. Wang, Z.P. Lu, Intermetallics 93 (2018) 269–273, doi:10.1016/j.intermet.2017.10.004.
[19] C.E. Slone, S. Chakraborty, J. Miao, E.P. George, M.J. Mills, S.R. Niezgoda, Acta Mater 158 (2018) 38–52, doi:10.1016/J.ACTAMAT.2018.07.028.
[20] O. Bouaziz, N. Guelton, Mater. Sci. Eng. A319-321 (2001) 246–249.
[21] W. Lu, X. Luo, Y. Yang, B. Huang, Mater. Express. 9 (2019) 291–298, doi:10.1166/mex.2019.1506.
[22] Z. Wu, W. Guo, K. Jin, J.D. Poplawsky, Y. Gao, H. Bei, J. Mater. Res. (2018) 1–9, doi:10.1557/jmr.2018.247.
[23] J. Miao, T. Guo, J. Ren, A. Zhang, B. Su, J. Meng, Vacuum 149 (2018) 324–330, doi:10.1016/j.vacuum.2018.01.012.
[24] J. Wang, H. Yang, H. Huang, J. Ruan, S. Ji, J. Alloys Compd. 798 (2019) 576–586, doi:10.1016/j.jallcom.2019.05.208.
[25] M.P. Agustianingrum, N. Park, S. Yoshida, N. Tsuji, J. Alloys Compd 781 (2018) 866–872, doi:10.1016/j.jallcom.2018.12.065.
[26] D. Lee, H.U. Jeong, K.H. Lee, J.B. Jeon, N. Park, Mater. Lett. 250 (2019) 127–130, doi:10.1016/j.matlet.2019.04.129.
[27] D. Lee, M.P. Agustianingrum, N. Park, N. Tsuji, J. Alloys Compd 800 (2019) 372–378, doi:10.1016/j.jallcom.2019.06.005.
[28] X.W. Liu, G. Laplanche, A. Kostka, S.G. Fries, J. Pfetzing-Micklich, G. Liu, E.P. George, J. Alloys Compd 775 (2019) 1068–1076, doi:10.1016/j.jallcom.2018.10.187.
[29] S.J. Patel, J.J. DeBarbadillo, B.A. Baker, R.D. Gollihue, Procedia Eng 55 (2013) 246–252, doi:10.1016/j.proeng.2013.03.250.
[30] C.E. Slone, E.P. George, M.J. Mills, J. Alloys Compd. In Press (2019).
[31] ASTM E112-13 ASTM, ASTM Int 1 (2013) 1–28, doi:10.1520/E0112-13..4.
[32] C.E. Slone, J. Miao, M.J. Mills, Scr. Mater. (2018) 155, doi:10.1016/j.scriptamat.2018.06.033.
[33] R.W. Hertzberg, R.P. Vinci, J.L. Hertzberg, Deformation and Fracture Mechanics of Engineering Materials, 5th ed., John Wiley & Sons, Inc., Hoboken, New Jersey, 2013, doi:10.1093/nq/s6-XII.297.185-c.
[34] H. Huang, X. Li, Z. Dong, W. Li, S. Huang, D. Meng, X. Lai, T. Liu, S. Zhu, L. Vitos, Acta Mater 149 (2018) 388–396, doi:10.1016/j.actamat.2018.02.037.
[35] R.C. Reed, The Superalloys: Fundamentals and Applications, Cambridge University Press, New York, 2006.
[36] S. Mahajan, G.Y. Chin, Acta Metall 21 (1973) 1353–1363.
[37] J.W. Christian, S. Mahajant, Prog. Mater. Sci. 39 (1995) 1–157.
[38] J. Kim, M. Kwon, B.C. De Cooman, Acta Mater 141 (2017) 444–455, doi:10.1016/j.actamat.2017.09.043.
[39] G. Kresse, J. Furthmüller, Phys. Rev. B. 54 (1996) 11169–11186, doi:10.1103/PhysRevB.54.11169.
[40] G. Kresse, D. Joubert, Phys. Rev. B. 59 (1999) 1758–1775, doi:10.1103/PhysRevB.59.1758.
[41] J.P. Perdew, K. Burke, M. Ernzerhof, Phys. Rev. Lett. 77 (1996) 3865–3868, doi:10.1103/PhysRevLett.77.3865.
[42] A. Zunger, S.-.H. Wei, L.G. Ferreira, J.E. Bernard, Phys. Rev. Lett. 65 (1990) 353–356, doi:10.1103/PhysRevLett.65.353.
[43] A. Van De Walle, P. Tiwary, M. De Jong, D.L. Olmsted, M. Asta, A. Dick, D. Shin, Y. Wang, L.Q. Chen, Z.K. Liu, Calphad Comput. Coupling Phase Diagrams Thermochem. 42 (2013) 13–18, doi:10.1016/j.calphad.2013.06.006.
[44] L. Delehouzee, A. Deruyttere, Acta Metall 15 (1967) 727–734.
[45] P.C. Gallagher, Metall. Trans. I (1970) 2429–2461.
[46] Z.Y. Liang, Y.Z. Li, M.X. Huang, Scr. Mater. 112 (2016) 28–31, doi:10.1016/j.scriptamat.2015.09.003.

[47] Z.C. Luo, M.X. Huang, Scr. Mater. 142 (2018) 28–31, doi:10.1016/j.scriptamat.2017.08.017.
[48] X. Fu, X. Wu, Q. Yu, Mater. Today Nano. 3 (2018) 48–53, doi:10.1016/j.mtnano.2018.11.004.
[49] J.D. Yoo, K. Park, Mater. Sci. Eng. A. 496 (2008) 417–424, doi:10.1016/j.msea.2008.05.042.
[50] E. Welsch, D. Ponge, S.M.H. Haghighat, S. Sandlobes, P. Choi, M. Herbig, S. Zaefferer, D. Raabe, Acta Mater 116 (2016) 188–199, doi:10.1016/j.actamat.2016.06.037.
[51] S.S. Sohn, A. Kwiatkowski, Y. Ikeda, F. Körmann, W. Lu, Adv. Mater. 31 (2019) 1–8, doi:10.1002/adma.201807142.
[52] L. Jiang, Y.P. Lu, M. Song, C. Lu, K. Sun, Z.Q. Cao, T.M. Wang, F. Gao, L.M. Wang, Scr. Mater. 165 (2019) 128–133, doi:10.1016/j.scriptamat.2019.02.038.